

1 **Modelling the anisotropic brine microstructure in first-year Arctic sea ice**

2

3 K.A. Jones¹, M. Ingham¹ and H. Eicken²

4 ¹School of Chemical & Physical Sciences, Victoria University of Wellington, PO Box
5 600, Wellington, New Zealand

6 ²Geophysical Institute, University of Alaska, Fairbanks, Alaska, USA

7

8 **Abstract**

9

10 Cross-borehole DC resistivity tomography has recently been used to monitor the
11 temporal variation of the anisotropic bulk electrical resistivity of first-year Arctic sea
12 ice during the period of spring warming. These measurements cannot be explained by
13 standard models of sea ice microstructure which treat the brine phase as isolated
14 ellipsoidal pores. A simple structural model which does satisfy the observed electrical
15 data shows that the brine phase must be connected both vertically and horizontally.
16 Calculation of the temporal and thermal evolution of the microstructure suggests that
17 although vertical connectivity is through pore tubes and sheets with widths of ~100
18 m, horizontal connectivity is through much thinner connections which are
19 interpreted as inter- and intragranular brine layers. As the temperature increases the
20 width of vertical channels increases smoothly. In contrast, at temperatures above
21 about -2 C there is a rapid increase in the thickness of horizontal connections which
22 we interpret as a change from conduction through intergranular brine layers to the
23 development of horizontal pores. The electrical data also broadly exhibit a percolation
24 transition predicted by mathematical models. However, the critical brine volume
25 fraction for vertical electrical connection is very small, while that for horizontal

26 electrical connection is derived to be about 0.5%. The difference between these and
27 the critical threshold of 5% for fluid permeability is presumed to arise because of the
28 strong dependence of the latter on brine channel width.

29

30 **1. Introduction**

31

32 Sea ice covers a large area of the high latitude oceans in the Arctic and Antarctic - at
33 maximum approximately 7% of the Earth's surface. As a consequence, sea ice plays
34 an important role in the global climate, reflecting a large fraction of incident solar
35 radiation, insulating the underlying ocean from the atmosphere, and, through the
36 rejection of salt into the ocean during ice formation, as an important driver of global
37 ocean circulation. The bulk properties of sea ice are primarily sensitive to the
38 geometry and connectivity of brine inclusions trapped within the solid ice matrix as
39 the sea ice forms. The size and connectivity of these inclusions vary greatly with
40 temperature and bulk salinity. At low temperatures inclusions tend to be smaller and
41 are presumed to be isolated within the ice matrix, whereas as sea ice warms they
42 expand and can ultimately form large connected networks. As individual brine
43 inclusions are preferentially vertically oriented, many of the physical properties of sea
44 ice are also anisotropic. Sea ice pore microstructure is therefore not only time and
45 temperature dependent but also highly complex. An understanding of the manner in
46 which this internal microstructure of sea ice changes in response to changes in
47 temperature is crucial for an understanding of the physical properties of the ice cover
48 and its interaction with the environment. For example, the existence and connectivity
49 of brine channels in the ice affects the transport of heat through the ice (Perovich,
50 1998; Weeks, 1998). Pringle et al. (2007) have suggested that internal brine motion
51 within the ice may contribute several percent to the overall heat flux, and in Arctic
52 summer sea ice fluid flow through pores constrains the pooling of surface meltwater
53 and hence ice albedo (Eicken et al., 2004). Fluid permeability is important for nutrient
54 transport through the ice (Fritsen et al., 1994), while brine inclusions also control the

55 manner in which the ice interacts with electromagnetic radiation (Hallikainen &
56 Winebrenner, 1992; Cherkaeva & Golden, 1998).

57

58 Recently Ingham et al. (2008) and Jones et al. (2010) have demonstrated that temporal
59 changes in the anisotropic microstructure of sea ice can be monitored *in-situ* using
60 cross-borehole dc electrical resistivity tomography. In particular, Jones et al. (2010)
61 presented 3-dimensional numerical models of the horizontal and vertical components
62 of sea ice resistivity derived from a suite of measurements made in first-year landfast
63 sea ice at Barrow, Alaska over the period April-June 2008 as the ice underwent spring
64 warming. These were derived from measurements made using four borehole
65 conductivity arrays deployed at the corners of a 1 x 1 m square in homogeneous,
66 undeformed landfast sea ice near Barrow, Alaska. A range of ancillary data was
67 obtained through ice coring and measurement of ice temperature profiles and ice
68 thickness at an adjacent instrumented site (Druckenmiller et al., 2009; Jones et al.,
69 2010). Measurements were made at roughly 2-week intervals during the latter stages
70 of the ice growth season beginning in early April, the transition into melt and into an
71 advanced stage of melt in mid-June. Jones et al. (2010) summarized their results as
72 plots of the formation factor (FF), the ratio of bulk resistivity to brine resistivity, as a
73 function of brine volume fraction (ϕ_b) within the sea ice, derived from measurements
74 of temperature and salinity of the ice. These are reproduced in Figure 1. The
75 formation factor can be related to brine volume fraction through an empirical
76 relationship (Archie, 1942)

$$77 \quad FF = \frac{\rho_{seaice}}{\rho_{brine}} = C\phi_b^{-m} \quad (1)$$

78 in which C and m are constants which may be regarded as functions of the
79 microstructure of the medium. In the absence of any changes in pore microstructure, a
80 log-log plot of formation factor against brine volume fraction yields a straight line of
81 slope $-m$. As reported by Jones et al. (2010) it is clear from Figure 1 that the measured
82 data largely follow this expected behaviour with a decrease in both the horizontal and
83 vertical formation factors associated with an increase in brine volume fraction as the
84 temperature increases. A sharp drop in the horizontal component of resistivity
85 between late May and mid-June appears as a discontinuity in the FF plot at a brine
86 volume fraction of approximately 10%. This may be indicative of a fundamental
87 change in the microstructure of the ice possibly related to the crossing of a percolation
88 threshold such as proposed by Golden et al. (1998, 2007).

89

90 The simple conclusion that can be drawn from Figure 1 is that the behaviour of the
91 bulk resistivity of sea ice as a function of brine volume fraction is that of a medium
92 which, up to a certain value of ϕ_b , has a fixed microstructure. That is, the geometry
93 and connectivity of brine pores within the ice remains essentially the same until a
94 point is reached at which the increase in brine volume ultimately leads to a significant
95 change in the morphology, size and connectivity of pores, possibly associated with a
96 percolation transition. In this paper we derive a model of the general form of sea ice
97 microstructure, and its evolution with time and temperature, which explains this
98 observed behaviour of the horizontal and vertical formation factors. Several authors
99 (e.g. Fricke, 1924; Archie, 1942; Hashin and Shtrikman, 1962; Tinga et al., 1973;
100 Vant et al. 1978; Timco, 1979; Sihvola and Kong, 1988; Chelidze and Gueguen,
101 1999; Grimm et al., 2008) have previously studied the electrical conductivity of
102 multiphase materials (sea ice included) and presented models based on mixture

theory. Many of these consider isolated spheroids of some form embedded in a background matrix. We initially discuss some of these models and consider how well they fit the observed resistivity data. We then develop our own simple structural model consisting of idealized cuboid inclusions of brine in a background ice matrix and show that it matches the thermal evolution of sea ice microstructure and its impact on resistivity.. Finally we consider how the observed variations in the formation factor may be related to percolation transitions.

110

111 **2. The effective electrical conductivity of mixtures**

112

Theories for the electrical properties of multiphase media were first considered by Maxwell (1873) with further developments by Wagner (1914) and Sillars (1937). Such treatments have generally had the aim of calculating the effective dielectric permittivity of a medium, although the results can be extended to calculate other physical properties. One of the earliest specific derivations of the effective electrical conductivity of a two-phase mixture was given by Fricke (1924). Fricke considered the electrical conductivity of a suspension of homogeneous non-polarisable spheroids with semi-axes a and b in which a is considered to be parallel to the direction of the electric field. He derived the conductivity σ of such a medium to be related to that of the host medium (σ_1) and of the spheroids (σ_2) by:

$$123 \quad \sigma = \sigma_1 \left(\frac{(1 - V_2)(\sigma_2 - \sigma_1) + \beta V_2 \sigma_2}{(1 - V_2)(\sigma_2 - \sigma_1) + \beta V_2 \sigma_1} \right) \quad (2)$$

124 Here V_2 is the volume concentration of the suspended medium (i.e. comparable in the
125 case of sea ice to the brine volume fraction), and β is given by

$$\beta = \frac{1}{3} \left\{ \frac{2}{1 + \left(\frac{\sigma_2}{\sigma_1} - 1 \right) \frac{M}{2}} + \frac{1}{1 + \left(\frac{\sigma_2}{\sigma_1} - 1 \right) (1 - M)} \right\} \left\{ \frac{\sigma_2}{\sigma_1} - 1 \right\}$$

The depolarization factor M depends upon the shape of the spheroids. For prolate

spheroids (i.e. $a > b$) it is given by $M = \frac{1}{\sin^2 \phi} - \frac{\cos^2 \phi}{2 \sin^3 \phi} \log \left(\frac{1 + \sin \phi}{1 - \sin \phi} \right)$ where

$\cos \phi = b/a$. For oblate spheroids ($b > a$) $M = \left(\phi - \frac{1}{2} \sin 2\phi \right) \cos \phi / \sin^3 \phi$, and

$\cos \phi = a/b$.

Following Fricke (1924), and also Beek (1967), Timco (1979) considered a medium

of conducting prolate spheroids in a poorly-conducting matrix as a model for the

vertical conductivity of sea ice. Timco gave the conductivity of this system of prolate

spheroids (with the electric field parallel to the long axis of the spheroid) as

$$\sigma = \frac{\sigma_1 [\sigma_1 + \{ A(1 - V_2) + V_2 \} (\sigma_2 - \sigma_1)]}{\sigma_1 + A(1 - V_2) (\sigma_2 - \sigma_1)} \quad (3)$$

where, again, σ_1 is the conductivity of the matrix (ice), σ_2 that of the spheroids (brine

inclusions), and V_2 is the brine volume fraction in parts per thousand. The factor A is

given by

$$A = \frac{-1}{(l/2b)^2 - 1} + \frac{(l/2b)}{\{(l/2b)^2 - 1\}^{3/2}} \ln \left[\frac{l}{2b} + \{(l/2b)^2 - 1\}^{1/2} \right]$$

where l is the length of a brine inclusion and b its average radius. From field

measurements Timco (1979) obtained values of vertical resistivity equal to 76 Ωm

and $V_2 = 63\%$. Assuming conductivities of the ice and brine of 3×10^{-5} S/m and 5 S/m,

respectively and a typical value for b of 0.046 mm, he then used (3) to derive an

average value for l of 1.7 cm.

146

147 Tinga et al. (1973) presented a further derivation of the effective dielectric
 148 permittivity of a two-phase mixture, again considering prolate ellipsoidal inclusions
 149 within a background matrix. Their result for the effective permittivity was
 150 subsequently used by Vant et al. (1978) in analysing dielectric measurements made on
 151 sea ice. The theory can also be used to express the effective bulk conductivity of such
 152 a mixture as:

$$153 \quad \sigma = \sigma_1 \left\{ 1 + \frac{V_2}{V_1} \frac{\sigma_2 - \sigma_1}{\sigma_1 + n_2(\sigma_2 - \sigma_1) - \left(\frac{n_1 V_2}{V_1} \right) (\sigma_2 - \sigma_1)} \right\} \quad (4)$$

154 where σ_1 and σ_2 are as above and V_2/V_1 is now the volume fraction of the inclusions.
 155 n_1 and n_2 are depolarisation factors which depend on the specific geometry of the
 156 inclusions and the orientation of the electric field. For ellipsoidal inclusions $n_1 = n_2 =$
 157 n (Vant et al., 1978) and therefore

$$158 \quad \sigma = \sigma_1 \left\{ 1 + \frac{V_2}{V_1} \frac{\sigma_2 - \sigma_1}{\sigma_1 + n(\sigma_2 - \sigma_1)(1 - (V_2/V_1))} \right\}$$

159 The depolarisation factors are given by

$$160 \quad n = \left(\frac{b}{a} \right)^2 \left(\frac{1}{4e^3} \right) \left(\frac{2e}{(b/a)^2} + \ln \frac{1-e}{1+e} \right)$$

161 when the electric field is parallel to the short axis (b) of the ellipsoids, and

$$162 \quad n = \left(\frac{b}{a} \right)^2 \left(\frac{1}{2e^3} \right) \left(-2e + \ln \frac{1+e}{1-e} \right)$$

163 when the electric field is parallel to the long axis (a) of the ellipsoids, e being the
 164 ellipsoid eccentricity defined by

$$165 \quad e = [1 - (b/a)^2]^{1/2}$$

166

167 The expressions given by Tinga et al. (1973) and Vant et al. (1978) allow for
168 consideration of electric fields applied both parallel and perpendicular to the long axis
169 of prolate ellipsoidal inclusions. Assuming, as did Timco (1979), that brine inclusions
170 may be modelled as prolate ellipsoids with the long axis vertically oriented, this
171 formulation allows both the horizontal and vertical resistivity of sea ice to be
172 investigated. Thus equation (4) gives the horizontal conductivity when the electric
173 field is parallel to the short axis of the ellipsoids and the vertical conductivity when
174 parallel to the long axis. The degree to which equation (4) is able to fit the observed
175 formation factor variation with brine volume fraction for differing ratios of the axes of
176 the embedded ellipsoids, is shown in Figure 2 assuming that the conductivities of ice
177 and brine take the values quoted by Timco (1979). Note that, with these conductivities
178 assumed, the results depend only the ratio b/a and not on the absolute dimensions of
179 the spheroids.

180

181 It can be seen from Figure 2 that a satisfactory fit to the vertical formation factor is
182 given for a value of $b/a \approx 0.004$. Lower values of the ratio underestimate the
183 formation factor, while higher values yield an overestimate. This is essentially the
184 same result obtained by Timco (1979) based on Fricke's theory. Assuming $b = 0.046$
185 mm, Timco's derived value for the length of the ellipsoidal inclusions yields $b/a =$
186 0.0054. However, despite the ability of equation (4) to fit the vertical formation factor
187 data, no value of b/a is able to fit the horizontal formation factor data unless a
188 significantly higher value (~ 0.001 S/m) is assumed for the ice conductivity. Although
189 there is evidence (e.g. Grimm et al., 2008) that high levels of impurities in the solid
190 ice phase may increase its conductivity markedly, impurity concentrations in “pure”

191 solid ice are typically expected, at most, to be at the level of parts per thousand
192 (Petrenko and Whitworth, 1999; Weeks, 2010). Thus such a high value for the ice
193 conductivity is considered unrealistic.

194 Grimm et al. (2008) compared measurements of electrical properties of ice-hydrate
195 binary systems with power law mixing models, which assume that each phase is
196 interconnected with an efficiency depending on an exponent m . Grimm et al. provided
197 the following expression for the general power law for two phases

$$198 \quad \sigma^{1/m} = \Phi_1 \sigma_1^{1/m} + (1 - \Phi_1) \sigma_2^{1/m} \quad (5)$$

199 where Φ_1 is the volume fraction of the medium with conductivity σ_1 . The exponent m
200 in this expression is commonly between 1 and 3. When $m = 1$ the Maxwell Garnett
201 expression

$$202 \quad \frac{\sigma - \sigma_1}{\sigma + 2\sigma_1} = (1 - \Phi_1) \frac{\sigma_2 - \sigma_1}{\sigma_2 + 2\sigma_1}$$

203 is approximated, while $m = 2$ or 3 , respectively lead to the refractive index model of
204 Birchak et al. (1974) and the Looyenga model (Looyenga, 1965). It is also worth
205 noting that if $\sigma_2 = 0$ equation (5) leads to Archie's Law with the empirical constant C
206 equal to one and σ_1 representing the conductivity of the more conductive phase.

207

208 Applying the above power-law mixing models to the observed formation factor data
209 for both the horizontal and vertical resistivity measurements shows that the best fit to
210 the horizontal resistivity data is given by $m = 3$, i.e., the Looyenga model.
211 Interestingly, this requires a much lower conductivity ($\sim 10^{-8}$ S/m) for the ice fraction
212 of the mixture than does the mixture model of Tinga et al. (1973). In contrast, the best
213 fit to the vertical resistivity data is achieved for $m = 2$, the refractive index model.

214 Nonetheless clearly no one model explains the observed variation with brine volume
215 fraction of both the horizontal and vertical formation factors.

216

217 **3. Development of a basic structural model**

218

219 The preceding discussion demonstrates that existing models for the bulk electrical
220 properties of a mixture are unable to simultaneously model satisfactorily both the
221 vertical and horizontal resistivity of sea ice. We therefore develop from first principles
222 a simple structural model that is able to reproduce the observed variation with brine
223 volume fraction of both the vertical and horizontal formation factors. Although the
224 resulting model, based on cubic structures, is unrealistic in terms of representing the
225 actual geometry of brine inclusions within sea ice it is effective in predicting both
226 how the size of pores must vary with time and temperature as the ice warms, and how
227 the interconnectivity of brine pores develops.

228

229 The initial model is based on a structure consisting of isolated cubes of material with a
230 conductivity of σ_2 (brine) within a matrix of a second material with a conductivity of
231 σ_1 (ice). Figure 3(a) shows a basic unit cell of this structure for which the conductivity
232 measured in the three different directions (x , y and z) will be the same. The bulk
233 conductivity (σ) of the material (the reciprocal of the bulk resistivity) can be found by
234 expressing the resistance presented to a current in any of these three directions in
235 terms of the parallel resistances of each possible current path. Hence, for example, in
236 any given direction in Figure 3(a) part of the total current passes solely through
237 material of conductivity σ_1 , and part through a combination of both σ_1 and σ_2 . In the
238 case of current travelling through both ice and brine the effective conductivity σ_e is

239 that of an element of cross-sectional area a^2 of which a length a has conductivity σ_2 ,
 240 and length b has conductivity σ_1 . Thus

$$241 \quad \sigma_e = \frac{(a+b)\sigma_1\sigma_2}{a\sigma_1 + b\sigma_2} \quad (6)$$

242 The effective bulk resistance of this section of material is

$$243 \quad R_e = \frac{a+b}{a^2\sigma_e} \quad (7)$$

244 and this is in parallel with a bulk resistance of

$$245 \quad R_1 = \frac{1}{\sigma_1} \frac{(a+b)}{(a+b)b + ab} \quad (8)$$

246 corresponding to the resistance of the remainder of the unit cell. The total bulk
 247 resistance of the unit cell in any direction may therefore be expressed as

$$248 \quad R_t = \frac{R_1 R_e}{R_1 + R_e} = \frac{1}{\sigma} \frac{(a+b)}{(a+b)^2}$$

249 which using (6), (7) and (8) gives the bulk conductivity of the structure shown in
 250 Figure 3(a) as

$$251 \quad \sigma = \left(1 - \frac{a^2}{(a+b)^2} \right) \sigma_1 + \frac{a^2}{(a+b)} \frac{\sigma_1\sigma_2}{(b\sigma_2 + a\sigma_1)} \quad (9)$$

252 The volume fraction of the material with a conductivity of σ_2 is given by

$$253 \quad \frac{V_2}{V} = \frac{a^3}{(a+b)^3} \quad (10)$$

254

255 For the structure shown in Figure 3(a) the isolated cubes represent brine inclusions
 256 and the background matrix solid ice. If the side of the unit cube $(a+b)$ is set to be
 257 constant, this confines the structure so that if the horizontal dimensions of the brine
 258 inclusions (a) increases the spacing between them (b) must decrease. The formation

259 factor (ρ/ρ_b) of models with different brine and ice conductivities can be calculated
260 over a range of brine volume fractions from equations (9) and (10). Using measured
261 temperature data (Druckenmiller et al., 2009) and the expression given by Morey et
262 al. (1984) it is possible to use the appropriate brine conductivity (σ_2) for each of the
263 observed data points in Figure 1. For any chosen value of σ_1 the resulting model
264 formation factors can then be compared to the measured data.

265 As the expected value for the conductivity of the solid ice matrix is not well
266 constrained a range of values for σ_1 have been considered. Calculation shows that it is
267 only when the resistivity of the solid ice matrix is as low as of the order of 1,000 Ωm
268 that a reasonable match between the magnitude of the calculated and observed
269 horizontal formation factors is obtained. This is essentially the same result, as shown
270 in Figure 2, found using the spheroidal inclusion model of Tinga et al. (1973) - to fit
271 the horizontal formation factor data requires an unrealistically low value for the
272 resistivity of the solid ice matrix. Furthermore, to fit the vertical formation factor data
273 would require an even lower value of ice resistivity of less than 75 Ωm . The low
274 values of ice resistivity required to fit the formation factor data can be concluded to
275 indicate the need for significant brine connectivity in both the vertical and horizontal
276 directions in order to match the resistivities measured by Jones et al. (2010).

277

278 In order to obtain a better match with the magnitude of the vertical formation factor
279 data we therefore consider a structure (Figure 3(b)) comprising vertical columns of
280 material with a conductivity of σ_2 (brine) within a matrix of a material with
281 conductivity of σ_1 (ice). For this structure the conductivity measured in the two
282 horizontal directions (x and y) will be the same, while that in the vertical direction (z)

will be higher. Hence $\sigma_x = \sigma_y = \sigma_H$ and $\sigma_z = \sigma_V$. Using the same considerations as for the bulk conductivity of the previous structure, expressions for the horizontal (σ_H) and vertical (σ_V) conductivities can be derived. The horizontal conductivity (σ_H) for this 'column' structure is given by

$$\sigma_H = \frac{b}{(a+b)}\sigma_1 + \frac{a\sigma_1\sigma_2}{b\sigma_2 + a\sigma_1} \quad (11)$$

while the vertical conductivity (σ_V) is

$$\sigma_V = \sigma_1 + \frac{a^2}{(a+b)^2}(\sigma_2 - \sigma_1) \quad (12)$$

The volume fraction of the material with conductivity of σ_2 is now given by

$$\frac{V_2}{V} = \frac{a^2(a+b)}{(a+b)^3} = \frac{a^2}{(a+b)^2} \quad (13)$$

As before the values for σ_2 for each data point obtained from the brine resistivities calculated by Jones et al. (2010) are used. The background ice matrix is taken to have $\sigma_1 = 0.0000001 \text{ Sm}^{-1}$, the dc conductivity of pure ice as noted by Petrenko and Whitworth (1999). If a sensible initial value for a is chosen and $a+b$ is set to be constant a value for b can now be deduced so that the model vertical formation factors (ρ_v/ρ_b), obtained using equation (12) and the relevant value of σ_2 , match the measured vertical formation factors. Using the derived values of a and b the brine volume fraction of the proposed ice structure can be found using (13). Note that in both (12) and (13) it is the ratio b/a which is important not the actual values of a and b . When this calculation is performed it is possible to reproduce the vertical formation factors obtained by Jones et al. (2010), however, these occur at brine volume fractions a factor of ~10-20 lower than in the observed data. This indicates the need for

305 additional brine inclusions within the structure. For the derived dimensions (a and b)
 306 of the column structure the horizontal formation factor can also be obtained from
 307 equation (11) and the value of σ_2 . Given the lack of connectivity of the conducting
 308 brine phase in the horizontal direction these derived values for the horizontal
 309 formation factor remain much larger than the observed values.

310

311 In a similar manner, to fit the observed horizontal resistivity formation factors it is
 312 possible to consider a structure consisting of horizontal tubes of a material with a
 313 conductivity of σ_2 within a matrix of conductivity of σ_1 . As Jones et al. (2010)
 314 considered horizontal isotropy within the ice it is necessary to have the same structure
 315 in both the x and y -directions of the model. A unit cell of such a structure is shown in
 316 Figure 3(c). For this structure it can be shown that the horizontal conductivity (σ_H) is
 317 given by

$$318 \quad \sigma_H = \frac{(a+b-c)}{(a+b)}\sigma_1 + \frac{ac}{(a+b)^2}\sigma_2 + \frac{(bc)}{(a+b)}\frac{\sigma_1\sigma_2}{(b\sigma_2 + a\sigma_1)} \quad (14)$$

319 the vertical conductivity (σ_V) by

$$320 \quad \sigma_V = \frac{b^2}{(a+b)^2}\sigma_1 + \frac{((a+b)^2 - b^2)}{(a+b)}\frac{\sigma_1\sigma_2}{((a+b-c)\sigma_2 + c\sigma_1)} \quad (15)$$

321 and the brine volume fraction by

$$322 \quad \frac{V_2}{V} = \frac{c((a+b)^2 - b^2)}{(a+b)^3} \quad (16)$$

323

324 Using the same values for a and b as derived for the 'column' structure discussed
 325 above, setting σ_2 to the brine resistivities calculated from the Jones et al. (2010) data
 326 and σ_1 to the dc conductivity of pure ice, equation (14) can be used to derive the

values of c , the vertical thickness of the horizontal tubes, which give a fit to the horizontal formation factor data. As for the 'column' model used to fit the vertical formation factor data it is possible to fit the observed horizontal data, but again with a brine volume fractions that are similarly much lower than for the observed data. As with the column structure and the vertical formation factor data this suggests that further brine inclusions are required. For the horizontal tube structure shown in Figure 3(c) the model vertical formation factor can be obtained from (15). In this case, lack of vertical connectivity means that the model values are too high.

To simultaneously fit both the vertical and horizontal formation factors the two previous structures can be combined to create a structure comprising of vertical columns of a material with conductivity of σ_2 and horizontal tubes of the same material within a matrix of conductivity σ_1 . A unit cell of this structure is shown in Figure 3(d). For this combined structure of tubes and columns the horizontal conductivity (σ_H) is given by

$$\sigma_H = \frac{b(a+b-c)}{(a+b)^2} \sigma_1 + \frac{ac}{(a+b)^2} \sigma_2 + \frac{a(a+b-c)+bc}{(a+b)} \frac{\sigma_1 \sigma_2}{b\sigma_2 + a\sigma_1} \quad (17)$$

and the vertical conductivity (σ_V) by

$$\sigma_V = \frac{b^2}{(a+b)^2} \sigma_1 + \frac{a^2}{(a+b)^2} \sigma_2 + \frac{2ab}{(a+b)} \frac{\sigma_1 \sigma_2}{(a+b-c)\sigma_2 + c\sigma_1} \quad (18)$$

while the volume fraction of the material with a conductivity of σ_2 is now given by

$$\frac{V_2}{V} = \frac{2abc + a^2(a+b)}{(a+b)^3} \quad (19)$$

349

350 Using the values for a , b and c as derived in the independent 'tube' and 'column'
 351 structures, setting σ_2 to the brine resistivities calculated by Jones et al. (2010) and σ_1
 352 to the dc conductivity of pure ice, equations (17) and (18) yields a fit to both the
 353 vertical and horizontal formation factors. However, the calculated brine volume
 354 fractions at which these formation factor values occur are still a factor of ~ 10 lower
 355 than in the observational data. Thus, although the structure shown in Figure 3(d)
 356 matches the observed formation factors it does not model the variation of these with
 357 brine volume fraction. The final stage in the development of a structural model that
 358 fully fits the observed variation of the formation factors with brine volume fraction is
 359 therefore the addition into the model of further brine inclusions.

360

361 One way to increase the brine volume fraction without significantly affecting the
 362 vertical or horizontal resistivities is to represent the overall effect of many small
 363 isolated brine inclusions by a single cube of brine of dimension d as illustrated in
 364 Figure 3(e). The components of resistivity of this new structure (tubes, cubes and
 365 columns of brine) are given by

$$\begin{aligned}
 366 \quad \sigma_H = & \frac{(b(a+b-c)-d^2)}{(a+b)^2} \sigma_1 + \frac{ac}{(a+b)^2} \sigma_2 \\
 367 & + \frac{(bc+a(a+b-c))}{(a+b)} \frac{\sigma_1 \sigma_2}{b\sigma_2 + a\sigma_1} \\
 368 & + \frac{d^2}{(a+b)} \frac{\sigma_1 \sigma_2}{(a+b-d)\sigma_2 + d\sigma_1} \quad (20)
 \end{aligned}$$

369 and

$$370 \quad \sigma_v = \frac{(b^2-d^2)}{(a+b)^2} \sigma_1 + \frac{a^2}{(a+b)^2} \sigma_2 + \frac{2ab}{(a+b)} \frac{\sigma_1 \sigma_2}{(a+b-c)\sigma_2 + c\sigma_1}$$

$$+ \frac{d^2}{(a+b)} \frac{\sigma_1 \sigma_2}{(a+b-d)\sigma_2 + d\sigma_1} \quad (21)$$

while the brine volume fraction is given by

$$\frac{V_b}{V} = \frac{2abc + a^2(a+b) + d^3}{(a+b)^3} \quad (22)$$

Knowing the difference between the brine volume fractions obtained from the data of Jones et al. (2010) (Figure 1) and the suggested column and tube structure in Figure 3(d), the required dimensions (d) of the additional brine inclusions can be found by equating this difference to the volume fraction of the cube giving

$$\Delta \frac{V_b}{V} = \frac{d^3}{(a+b)^3} \Rightarrow d = \sqrt[3]{\left(\Delta \frac{V_b}{V} \right) (a+b)^3}$$

Using the values for a , b and c found from the 'tube' and 'column' structures, the value of d obtained from the expression above, setting σ_2 to the observed brine resistivities and σ_1 to the dc conductivity of pure ice, equations (20) and (21) can be used to fit the vertical and horizontal formation factors. Such a structure comprised of columns, tubes and cubes of brine can be constructed so that the variation of the formation factors with brine volume fraction closely fit the observed data of Jones et al. (2010). Indeed, differences between the values obtained from the model structures and the values obtained from the measured data are less than 1%.

The data are clearly well fit by this structure using brine resistivities calculated from measured temperature data, and the estimate of the conductivity of pure ice as given by Petrenko and Whitworth (1999). Nevertheless, as noted above, the conductivity of the solid ice matrix is not well constrained. It is important therefore to consider how changing the conductivity of the ice affects the bulk resistivities calculated from the

model structure. By taking average values for the conductivity of the brine and the dimensions of the structure (a , b , c , and d) equations (20) and (21) can be used to find the horizontal and vertical conductivity of the structure for different values of the conductivity of the ice matrix. Figure 4 shows the calculated bulk horizontal and vertical conductivities of the medium for different assumed conductivities of the ice matrix. It can be seen that neither the calculated horizontal nor vertical effective conductivities change significantly with increasing ice conductivity until that conductivity reaches 0.001 Sm^{-1} (corresponding to a resistivity of $1000 \text{ }\Omega\text{m}$). As has been indicated previously, since most of the salt is excluded from the ice crystal lattice as seawater freezes, such a low value for the resistivity of the solid ice is considered unrealistic. Thus the derived model results are robust with respect to changes of the conductivity of the ice within a reasonable range of expected values.

4. Results: Variations in the relative dimensions of brine inclusions

It is the relative sizes of the dimensions a , b , c and d that are important in deriving a model that fits the observed data. If all dimensions are multiplied by an arbitrary value the calculated conductivities will remain the same. As individual points in the plots of formation factor against brine volume fraction relate to not only different measurement dates, but also different depths in the ice, this allows some assessment of how the dimensions and connectivity of brine inclusions vary not only with time and within the ice column, but also with temperature. Initially we consider changes in the relative dimensions of the structural features. Subsequently we relate the relative dimensions of features to actual likely dimensions of brine channels and pores as suggested by previous studies.

419

420

421 Shown in Figure 5 are the variations in the dimensions a , b , c and d (relative to the
422 smallest value of a derived for the earliest set of measurements on April 7-9, 2008) as
423 a function of depth in the ice for each of the six measurement dates reported by Jones
424 et al. (2010). The temperature profiles through the ice on each of these dates are also
425 shown in Figure 5, while the variations in the calculated relative dimensions are shown
426 as a function of temperature in Figure 6. It is shown in both Figures 5 and 6 that the
427 mean horizontal dimension (a) of the idealized brine columns increases gradually by a
428 factor of 2 to 3 as the ice warms from April to June. The column widths are also
429 greater at the bottom of the ice, closer to the ice-water interface where the temperature
430 remained at approximately -2°C during the measurement period (Petrich et al.,
431 unpublished data available online at aoncadis.org and
432 seaice.alaska.edu/gi/data/barrow_massbalance; see also Druckenmiller et al., 2009).
433 Equally, as the upper parts of the ice warm in response to rising air temperatures and
434 solar heating in mid- to late May, there is an increase in a in the near-surface. The
435 obvious exception to this trend is for the data from 16-17 June where, although there
436 is a continuing increase in a , thinner columns occur at the surface and base of the ice.
437 The variation in the separation between the columns (b) is the mirror image of the
438 variation in a . As $(a + b)$ is constrained to be constant this is as expected. The
439 separation of columns is approximately 17 to 20 times larger than their width. In
440 contrast, the thickness of the horizontal tubes (c) is an order of magnitude smaller than
441 a and shows only a slight increase with temperature between the initial measurements
442 in early April and those in late May. However, there is subsequently a large jump in c
443 between the 28-29 May and 16-17 June when temperatures within the ice rise above -

2 C. In contrast to the occurrence of clear trends in a , b and c , there is no obvious trend in the dimension (d) of the isolated inclusions of brine between measurement sets (Figure 5). The collated data (Figure 6) do suggest a slight increase in dimension with rising temperature. This dimension is between 7 and 10 times that of the vertical columns.

5. Discussion: Pore evolution derived from the geoelectric microstructural model and borehole data

While the geoelectric microstructural model introduced in Section 3 is based on observations of pore microstructure and has been constrained by in-situ conductivity measurements, it simplifies microstructure by assuming a monodisperse distribution of pores of idealized shape. In order to arrive at estimates of specific pore sizes we need to first consider the model results in the context of typical sea-ice pore inventories and then relate them to available data on pore sizes obtained through other means. As typical of Arctic congelation sea ice (Weeks, 2010), landfast ice at the Barrow field site comprises two major classes of brine inclusions, illustrated in Figure 7(a) and (b). Brine channels are typically several mm to >1 cm in diameter and extend for several cm to decimeters downcore (as evident at the field site, Fig. 7(a)). Due to the homogeneity of the sampled ice cover and little interannual variability at the field site (Druckenmiller et al., 2009), we can relate measurements made in 2008 to pore structures studied in depth in past years. This earlier work showed that such large brine channels typically occur at spacings of 10 to 20 cm, and account for a total brine volume fraction of at most 1 to 2 % (Cole and Shapiro, 1998; Miner et al., unpubl.

468 data). Such findings are in line with work at other sites and in the laboratory
469 (Wakatsuchi and Kawamura, 1987).

470

471 Most of the brine in the ice studied is contained in smaller pores that form initially as
472 brine layers in the interstices between ice lamellae protruding from the base of the ice
473 cover (Fig. 7(b)). Higher up in the ice, owing to lower temperatures, such inclusions
474 segregate into brine tubes and strings of individual brine pockets, reconnecting as the
475 ice warms at the end of the ice-growth season (Light et al., 2003; Pringle et al., 2009).
476 The width of the ice lamellae, and hence the spacing of brine layers or brine tubes, has
477 been found to range between 0.4 and 1.0 mm in comparable Arctic sea ice by Nakawo
478 and Sinha (1984). Similar ranges are reported by Weeks (2010) for sea ice in both
479 polar regions, with brine layers at most 0.1 mm thick and up to several mm long.

480

481 Along the same lines, Petrich et al. (2006) who carried out computational fluid
482 dynamics simulations of fluid permeability in sea ice noted that brine tubes tend to
483 break into isolated inclusions when their width is less than 70 μm , and found that the
484 spacing of brine layers (or plates) in a sandwich model of sea ice needed to be ~ 360
485 μm to be able to simulate the proposed percolation threshold for permeability. Optical
486 microscopy measurements on vertical thin sections by Light et al. (2003) also
487 suggested that the width of brine tubes is $\sim 100 \mu\text{m}$, which is in line with thin section
488 analysis completed on samples obtained at Barrow (Figure 7(c), Junge et al., 2001).
489 Furthermore, Light et al. (2003) observed increases of the order of a factor of 2 in the
490 width of such tubes when sections were warmed from -15°C to -2°C . Similar values
491 were also quoted by Addison (1969) in interpreting electrical permittivity data.

492

493 Given this agreement between a variety of different types of studies, it seems
494 reasonable to take the basic width of the vertical columns (a) in the structural model
495 as being ~ 100 μm and assuming that these columns correspond to both the smaller
496 brine tubes or layers (which make up the bulk of the pore space) and the larger brine
497 channels which account for a smaller fraction of the total liquid volume in the ice.
498 Given the derived relative dimensions this suggests that the separation of vertical
499 columns (b) is ~ 2 mm, the thickness of the horizontal tubes (c) through most of the
500 measurement period is ~ 10 μm , and the dimension of the isolated brine pockets (d) is
501 ~ 0.7 - 0.8 mm.

502

503 While few studies have examined the small-scale pores in detail, it should be noted
504 that the much smaller width of horizontal connecting tubes (i.e., dimension c) does
505 match thin-section microscopy studies in the same type of ice at the same field site,
506 illustrated in Figure 7(c). Thus, it is common to find horizontally connecting pores
507 few micrometers to at most few tens of micrometers in width that connect the primary
508 vertically oriented brine layers or tubes discussed above (see also Cole et al., 2002).

509

510 The calculated spacing between the columns, i.e., the brine layers or tubes, is
511 consistent with that for brine layers within individual columnar sea ice crystals. In
512 reviewing the literature and interpreting field-based nuclear magnetic resonance
513 (NMR) data Callaghan et al. (1999) also give ~ 1 mm for this spacing, with a similar
514 value reported by Shokr and Sinha (1994). Although the decrease in spacing (b) with
515 rising temperature (Figure 6) is controlled by the constancy of $(a + b)$ in the
516 modelling, it is likely to represent an actual increase in density of columnar tubes with
517 temperature. For example, Light et al. (2003) reported that vertical chains of isolated

518 brine inclusions were observed to coalesce as the ice warmed, effectively creating
519 new vertical channels – and by implication decreasing the separation of vertical
520 channels. This was also found in an analysis of ice of comparable microstructure
521 obtained near the Barrow field site in 1999 and analyzed using magnetic resonance
522 imaging (MRI) techniques (Eicken et al., 2000).

523

524 Moreover, the derived thicknesses (c) of the horizontal tubes are comparable with
525 measurements of the thickness of intragranular brine veins and layers obtained from
526 optical microscopy (Figure 7(c); Junge et al., 2001). This may indicate differences in
527 the nature of conductivity pathways in the horizontal as compared to the vertical
528 direction. It has previously been suggested that dc conductivity in sea ice may be
529 controlled by the brine distribution existing at grain boundaries (Toyama et al., 2001),
530 similar to connected liquid veins at triple junctions in glacial ice (Wolff et al., 1997).
531 Light et al. (2003) commented on the potential formation, during rapid cooling of the
532 ice, of microcracks around inclusions. These were suggested to provide channels for
533 hydraulic, and presumably electrical, contact between otherwise isolated pores. The
534 significant increase in the size of the horizontal tubes on the 16-17 June as the ice
535 reaches temperatures in excess of -2 C may thus reflect a change in the nature of
536 horizontal conduction. However, stratigraphic analysis of cores taken in the field in
537 late May and early June also indicates that larger brine layers (mm to cm-sized) that
538 formed during warming and meltwater drainage in the ice may also have contributed
539 to the order of magnitude increase in the thickness of horizontal brine inclusions.

540

541 Various authors (e.g. Bock & Eicken, 2005; Cole & Shapiro, 1998; Eicken et al.,
542 2000; Light et al., 2003; Perovich & Gow, 1996; Petrich et al., 2006) have discussed

543 the size distribution of isolated brine inclusions. In general these authors quote typical
544 cross-sectional areas in the range of 0.02 – 0.5 mm², depending on the resolution of
545 the study in question. The majority of these quoted values are smaller than the ~0.5-
546 0.6 mm² indicated by the calculated dimension (d) of the isolated brine pockets in the
547 structural model. Such a discrepancy can readily be accounted for by the fact that the
548 model idealises all additional brine other than that in the vertical and horizontal tubes
549 or channels as being in a single pore rather than being contained in a larger number of
550 smaller pores.

551

552 While the assumption of monodisperse brine inclusions is simplistic, data collected at
553 the field site and a review of the literature suggests that prior to the onset of internal
554 melt the bulk, i.e., typically more than three-quarters and often more than 90%, of the
555 total brine volume resides within the small-scale brine layers, brine tubes and isolated
556 brine pockets; the remainder of the brine is contained within larger brine inclusions
557 such as brine channels (Wakatsuchi and Kawamura, 1987; Eicken et al., 2000; Miner
558 et al., unpubl. observations). Hence, it is not clear to what an extent the data on
559 increases in pore dimensions are skewed by potential disproportionate increases in
560 pore size and connectivity of either the small- or large-scale pore fraction. However,
561 MRI data for ice obtained at a nearby site in earlier years indicate that for pore linear
562 dimensions between 0.7 and 6 mm there are no statistically significant differences in
563 the change in pore dimensions along the three principal axes between the entire data
564 set and the upper ten-percentile as the ice warms from –21 °C to –6 °C (Eicken et al.,
565 2000). The only indication of disproportionate contribution of large (several mm to
566 cm-sized) pores to observed changes in resistivity is for the increase in horizontal tube
567 or layer thickness by almost an order of magnitude between late May and mid-June.

568 This is also borne out by the increase in c shown in Figure 6c as a function of
569 temperature. In part, this increase may be the result of the development of horizontal
570 layers of mm- to cm-sized pores in the upper half of the ice cover as a result of
571 internal heating and melt in the advanced stages of melt, as identified in cores drilled
572 near the site.

573

574 In summary, the basic two phase, composite structure that has been developed in the
575 model presented here is able to reproduce the observed bulk resistivities in both the
576 horizontal and vertical directions, and their dependence on brine volume fraction.
577 Although the assumed structure of vertical and horizontal brine connections, and
578 isolated brine cubes is a highly simplistic idealization of a more complex
579 microstructure, it yields a coherent and consistent picture of the aggregate
580 microstructure of brine inclusions and their connectivity as a function of ice
581 temperature and ice developmental stage within landfast first-year Arctic sea ice.

582

583 **6. Discussion: Percolation models**

584

585 Both Ingham et al. (2008) and Jones et al. (2010) speculated that the rapid decrease in
586 the horizontal component of bulk resistivity (ρ_H) observed late in the melt season
587 might indicate a percolation transition. As is clear from the above discussion we now
588 propose that this change results from a change in the nature of horizontal conduction
589 from being through grain boundary conduction to through horizontal pores. Although
590 this observed change is interpreted not to be related to the crossing of a percolation
591 threshold in brine volume fraction, it is worthwhile considering what indication of any

592 percolation transition in the electrical properties of the sea ice the dataset as a whole is
593 able to provide.

594

595 Percolation theory describes the connectivity of two-phase systems (Balberg, 2009) in
596 which the bulk physical properties of the system are dominated by those of one phase
597 below a certain threshold, while above the threshold the physical properties of the
598 second phase dominate. Sea ice may be regarded as a largely two-phase system for
599 which many of the transport properties may exhibit percolation transitions. For
600 example, it was first noted by Cox & Weeks (1975) that sea ice is effectively
601 impermeable to fluid flow for brine volume fractions of about 5%, but that above this
602 threshold ice is permeable. Golden et al. (1998, 2006, 2007) and Golden (2001, 2003)
603 have proposed percolation theory as an explanation for this observed behaviour which
604 typically corresponds to a salinity of 5 ‰ and a temperature of -5 C. Golden et al.
605 (2007) have proposed that for brine volume fractions above a critical value of ϕ_c the
606 permeability can be expressed as

$$607 \quad k_v = k(\phi_b - \phi_c)^2 \quad (23)$$

608 where k is a scaling factor and the critical exponent 2 is appropriate for a 3-
609 dimensional medium such as sea ice with log-normally distributed brine inclusions
610 (Golden et al., 2007; Berkowitz & Balberg, 1992).

611

612 The critical exponent for fluid permeability is believed to be universal, depending
613 only on the dimension, and equal to that for electrical conduction. A similar
614 relationship is thus expected to hold for the bulk electrical conductivity and it is
615 therefore of interest to see how well such a predicted relationship fits the observed
616 formation factor data. In terms of formation factor (FF), which is based on resistivity

617 (the reciprocal of conductivity) rather than conductivity itself, the expected
618 relationship takes the form

$$619 \quad FF = FF_o (\phi_b - \phi_c)^{-2} \quad (24)$$

620 Although the critical brine volume fraction for fluid permeability is recognized as 5%,
621 as has been noted by Golden et al. (2006) whereas the electrical conductivity is a
622 property of a material, the corresponding fluid conductivity depends on the
623 dimensions of the conductor. Thus there seems to be no *a priori* reason to assume that
624 the percolation threshold for electrical conductivity should similarly be 5%.

625
626 The possible fit of expressions of the form of (24) to both the vertical and horizontal
627 formation factor data has been investigated. The data obtained by Jones et al. (2010)
628 extend down to a minimum brine volume fraction of 3.3% and the vast majority of the
629 data correspond to brine volume fractions greater than 5%. To attempt to improve the
630 ability to obtain reasonably well constrained numerical values for the parameters ϕ_c
631 and FF_o the horizontal formation factor data have been supplemented by
632 measurements at lower brine volume fractions (down to 2.5%) made by Ingham et al.
633 (2008). Table 1 shows, for different possible values of critical brine volume fraction
634 ϕ_c , the derived value of the scaling factor FF_o which gives the minimum root mean
635 square misfit (measured in terms of the logarithm of the formation factor) to the
636 measured data. Figure 8 illustrates the fit which several of these combinations of ϕ_c
637 and FF_o give to the data. Both Table 1 and Figure 8 demonstrate that although it is
638 possible to fit both the vertical and horizontal formation factor data with expressions
639 of the appropriate form, the natural scatter in the observed data makes resolution of
640 the best fitting parameters difficult. Nonetheless some broad conclusions may be
641 drawn. For example, it appears from both Table 1 and Figure 8 that if the vertical

642 formation factor data are to be represented by (24) then the best fit to the data is given
643 by a very small critical brine volume fraction, significantly less than 1%. In contrast
644 the horizontal formation factor data are best fit with a critical brine volume fraction of
645 0.5-1%. In both cases it is clear from Figure 8 that the measured misfit is heavily
646 biased by how well the function is able to fit the data at low and high values of ϕ_c . It is
647 also likely that the apparent discontinuity in the horizontal formation factor at brine
648 volume fractions of about 10%, noted by Jones et al. (2010), is not itself indicative of
649 a percolation transition. Rather it is likely that it results from the data gap between
650 their measurement dates in late May and mid-June.

651

652

653 Although these deductions are somewhat speculative, the results appear at least
654 conceptually consistent with the results of the microstructural modelling. The
655 existence of vertically oriented brine channels of relatively large width (~ 100 μm)
656 compared to the absence of such channels horizontally, is consistent with the
657 horizontal resistivity having a larger critical brine volume fraction. It has been
658 observed, for example, that at lower temperatures grain boundary brine films, such as
659 proposed to explain the horizontal resistivity data, tend to be confined exclusively to
660 high angle grain boundaries (Grimm et al., 2008) and connectivity between films is
661 cut off. A lower vertical critical brine volume fraction is also consistent with the
662 observation by Light et al. (2003) that the majority of the brine volume is contained in
663 vertical channels. Thus during warming of sea ice brine appears preferentially in
664 vertical channels which form a connected network at lower brine volume fractions
665 than do inter- and intragranular horizontal films. However, recent work by Pringle et
666 al. (2009) indicates that the morphology of brine layers and brine tubes in ice that has

667 been cooled and then rewarmed (at temperatures comparable to those observed in the
668 field) is in fact much more complicated and may not conform with simple geometric
669 models (including the assumption of tubes or even planar layers). Further work is
670 needed to quantify the morphology of these inclusions and relate them to
671 microstructural models extant in the literature.

672

673 The difference between the critical brine volume fractions proposed for electrical
674 connection and that of 5% observed for fluid permeability is presumably related to the
675 strong additional dependence of the latter on the dimensions of constrictions along the
676 direction of flow. However, few measurements exist of the bulk resistivity of sea ice
677 at very low brine volume fractions. Confirmation or otherwise of the indicated critical
678 thresholds will require such measurements.

679

680 **7. Conclusions**

681

682 The structural modelling presented here allows us to present the first coherent
683 description of the temporal and thermal evolution of sea ice microstructure based on
684 *in-situ* measurements of a physical property of the ice.

685

686 First and foremost, accepted values for the resistivity of the ice phase in sea ice
687 indicate that to explain the observed resistivity data of Jones et al. (2010) at lower
688 temperatures there must be both vertical and horizontal electrical connectivity through
689 the brine phase. The structural modelling suggests that vertically this occurs
690 predominantly through brine channels with dimensions of the order of 100 μm , such
691 as have been observed to exist in optical microscopy measurements. However, as the

692 modelling uses a very simplistic and idealised structure, it can be assumed that in
693 reality such vertical brine channels have a finite length. The necessary electrical
694 connection between individual channels is therefore likely to occur through brine
695 films and channels of much smaller thickness which exist along crystal/grain
696 boundaries. The existence of two populations of pores of different sizes was suggested
697 by Callaghan et al. (1999) on the basis of NMR measurements of brine diffusivity.
698 These smaller size inter- and/or intragranular brine layers are similarly believed to
699 give the necessary electrical connectivity in the horizontal direction, and were the
700 only kind of pores identified by Callaghan et al. in horizontal orientations. Additional
701 isolated brine pores contribute significantly to the overall brine volume fraction.

702

703 As the ice warms the dimensions of vertically oriented channels gradually increase.
704 Although vertical fluid permeability is believed to undergo a percolation transition at
705 brine volume fractions of 5%, fitting the requisite mathematical form to the resistivity
706 data suggests that such a transition in vertical electrical conductivity occurs at a much
707 smaller brine volume fraction. As a result although the bulk vertical resistivity
708 decreases for brine volume fractions greater than 5%, it does so smoothly rather than
709 in a discontinuous fashion. In contrast, a significant increase in the dimensions of
710 horizontal tubes is deduced to occur as temperatures rise above -2 C. This was
711 initially proposed by Ingham et al. (2008) to represent a percolation transition in
712 horizontal resistivity. However, we now suggest that this change represents a
713 transition from horizontal electrical connection predominantly through grain boundary
714 films of brine to connection through more extensive pores, equivalent to the brine
715 channels that dominate vertical resistivity at much lower temperatures. Any actual

percolation transition in horizontal resistivity is believed to occur at much smaller brine volume fractions below which grain boundary connectivity is lost.

Although the evolution of sea ice microstructure described here is specifically related to measurements of electrical resistivity, it represents a step in developing an integrated understanding of the evolution of other physical properties which have a more direct impact on the important role that sea ice plays in the global climate system.

Acknowledgements

KJ is supported by a Victoria University of Wellington Postgraduate Assistantship. We acknowledge financial support through NSF Office of Polar Programs Grants ARC-0620124 and 0934683.

References

Addison, J. R., 1969, Electrical properties of saline ice, *Journal of Applied Physics*, 40, 3105-3114.

Archie, G.E., 1942, The electrical resistivity log as an aid in determining some reservoir characteristics. *Trans. Am. Inst. Min. Metall. Eng.*, 146, 54–62.

Balberg, I, 2009, Tunnelling and percolation in lattices and the continuum, *J. Phys. D: Appl. Phys.*, 42, doi:10.1088/0022-3727/42/6/064003.

741

742 Beek, L. K. H. van., 1967, Dielectric behaviour of heterogeneous systems, *Progress*
743 *in Dielectrics*, 7, 69-114.

744

745 Berkowitz, B. & I. Balberg, 1992, Percolation approach to the problem of hydraulic
746 conductivity in porous media, *Transport Porous Media*, 9, 275-286.

747

748 Birchak, J. R., L. G. Gardner, J. W. Hipp, and J. M. Victor, 1974, High dielectric
749 constant microwave probes for sensing soil moisture, *Proceedings of the IEEE*, 62(1),
750 93-98.

751

752 Bock, C. and H. Eicken, 2005, A magnetic resonance study of temperature-dependent
753 microstructural evolution and self-diffusion of water in Arctic first-year sea ice, *J.*
754 *Glaciology*, 40, 1-6.

755

756 Callaghan, P.T., R. Dykstra, C.D. Eccles, T.G. Haskell and J.D. Seymour, 1999, A
757 nuclear magnetic resonance study of Antarctic sea ice brine diffusivity, *Cold Reg. Sci.*
758 *Technol.*, 29, 153-171.

759

760 Chelidze, T. L. and Y. Gueguen, 1999, Electrical spectroscopy of porous rocks: a
761 review – I. Theoretical models, *Geophys. J. Int.*, 137, 1-15.

762

763 Cherkaeva, E. and K.M. Golden, 1998, Inverse bounds for microstructural parameters
764 of composite media derived from complex permittivity measurements, *Waves in*
765 *Random Media*, 8, 437-450.

766

767 Cole, D.M. and L.H. Shapiro, 1998, Observations of brine drainage networks and
768 microstructure of first-year sea ice, *J. Geophys. Res.*, *103*, 21739-21750.

769

770 Cole, D. M., H. Eicken, L. H. Shapiro, and K. Frey, 2002, Some observations of high
771 porosity layers and brine drainage features in first-year sea ice. Proceedings of the
772 16th IAHR International Symposium on Ice: Ice in the Environment, Dunedin, New
773 Zealand, 2nd-6th Dec. 2002, vol. 2, 179-186.

774

775 Cox, G. F. N., and W. F. Weeks, 1975, Brine drainage and initial salt entrapment in
776 sodium chloride ice, *CRREL Res. Rep.*, 345.

777

778 Cox, G. F. N. and W. F. Weeks, 1983, Equations for determining the gas and brine
779 volumes in sea-ice samples: *J. Glaciol.*, *29*, 306–316.

780

781 Druckenmiller, M. L., H. Eicken, D. J. Pringle, C. C. Williams, and M. A. Johnson
782 (2009), Towards an integrated coastal sea-ice observatory: System components and a
783 case study at Barrow, Alaska, *Cold Reg. Sci. Tech.*, *56*, 61-72.

784

785 Eicken, H., T. C. Grenfell, D. K. Perovich, J. A. Richter-Menge, and K. Frey, 2004,
786 Hydraulic controls of summer Arctic pack ice albedo, *J. Geophys. Res.*, *109*,
787 doi:10.1029/2003JC001989.

788

789 Eicken, H., C. Bock, R. Wittig, H. Miller and H.-O. Poertner, 2000, Magnetic
790 resonance imaging of sea ice pore fluids: methods and thermal evolution of pore
791 microstructure, *Cold Reg. Sci. Technol.*, 31, 207–225.
792
793 Fricke, H., 1924, A mathematical treatment of the electric conductivity and capacity
794 of disperse systems I: The electric conductivity of a suspension of homogeneous
795 spheroids, *Phys. Rev.*, 4, 575-587
796
797 Fritsen, C.H., V.I. Lytle, S.F. Ackley, S.F. and C.W. Sullivan, 1994, Autumn bloom
798 of Antarctic pack-ice algae, *Science*, 266, 782-784.
799
800 Golden, K.M., S.F. Ackley and V.I. Lytle, 1998, The percolation phase transition in
801 sea ice. *Science*, 282, 2238-2241.
802
803 Golden, K.M. 2001, Brine percolation and the transport properties of sea ice, *Annals*
804 *of Glaciology*, 33, 28-36.
805
806 Golden, K.M., 2003, Critical behavior of transport in sea ice, *Physica B*, 338, 274-
807 283.
808
809 Golden, K.M., A.L. Heaton, H. Eicken and V.I. Lytle, 2006, Void bounds for fluid
810 transport in sea ice, *Mech. Mater.*, 38, 801-817.
811

812 Golden, K. M., H. Eicken, A.L. Heaton, J. Miner, D.J. Pringle and J. Zhu, 2007,
813 Thermal evolution of permeability and microstructure in sea ice, *Geophys. Res. Lett.*,
814 34, L16501, doi:10.1029/2007GL030447
815
816 Grimm, R. E., D. E. Stillman, S. F. Dec and M. A. Bullock, 2008, Low-Frequency
817 Electrical Properties of Polycrystalline Saline Ice and Salt Hydrates, *J. Phys. Chem. B*,
818 112, 15382–15390.
819
820 Hallikainen, M. and D.P. Winebrenner, 1992, The physical basis for sea ice remote
821 sensing, in *Microwave Remote Sensing of Sea Ice*, edited by F.D. Carsey, pp. 29-46,
822 Geophysical Monograph, vol. 68, American Geophysical Union, Washington.
823
824 Hashin, Z. and S. Shtrikman, 1962, A variational approach to the theory of the
825 effective magnetic permeability of multiphase materials, *J. Appl. Phys.*, 33, 3125-
826 3131.
827
828 Ingham, M., D. Pringle, and H. Eicken, 2008, Cross-borehole resistivity tomography
829 of sea ice, *Cold Reg. Sci. Technol.*, 52, 263-277.
830
831 Jones, K. A., M. Ingham, D. J. Pringle, and H. Eicken, 2010, Temporal variations in
832 sea ice resistivity: resolving anisotropic microstructure through cross-borehole dc
833 resistivity tomography, *J. Geophys. Res.*, 115, C11023, doi:10.1029/2009JC006049.
834

835 Junge, K., C. Krembs, J. Deming, A. Stierle and H. Eicken, 2001, A microscopic
836 approach to investigate bacteria under in situ conditions in sea-ice samples, *Annals.*
837 *Glaciology*, 33, 304-310.

838

839 Light, B., G.A. Maykut and T.C. Grenfell, 2003, Effects of temperature on the
840 microstructure of first-year Arctic sea ice, , *J. Geophys. Res.*, 108(C2), 3051,
841 doi:10.1029/2001JC000887.

842

843 Looyenga, H., 1965. Dielectric constant of heterogeneous mixtures, *physica*, 31, 401-
844 406.

845

846 Mathews, F. S. and F. C. Clarke, 1963, The electrical, structural and topographical
847 characteristics of Arctic sea ice, *DECO ELECTRONICS CAMBRIDGE MA - Defense*
848 *Technical Information Center*.

849

850 Maxwell, J., 1873, *A treatise on electricity and magnetism*, Clarendon Press.

851

852 Morey, R. M., A. Kovacs, and G. F. N. Cox, 1984, Electromagnetic properties of sea
853 ice, *Cold Reg. Sci. Technol.*, 9, 53-75.

854

855 Petrich, C., P. J. Langhorne, and Z. F. Sun, 2006, Modelling the interrelationships
856 between permeability, effective porosity and total porosity in sea ice, *Cold Reg. Sci.*
857 *Technol.*, 44, 131-44.

858

859 Perovich, D.K., 1998, Optical properties of sea ice, in: *Physics of Ice-Covered seas*,
860 editor M. Lepparanta, pp. 195-230, Springer-Verlag, New York.

861

862 Perovich, D.K. and A.J. Gow, 1996, A quantitative description of sea ice inclusions,
863 *J. Geophys. Res.*, *101*, C8, 18327-18343.

864

865 Petrenko, V.F. and R.W. Whitworth, 1999. *Physics of ice*, Oxford University Press.

866

867 Pringle, D. J., J. Miner, H. Eicken, and K. M. Golden, 2009, Pore space percolation in
868 sea ice single crystals, *J. Geophys. Res.*, *114*, C12017,
869 doi:10.1029/2008JC005145.

870

871 Pringle, D.J., H. Eicken, H.J. Trodahl, and L.G.E. Backstrom, 2007, Thermal
872 conductivity of landfast Antarctic and Arctic sea ice, *J. Geophys. Res.*, *112*, C04017,
873 doi:10.1029/2006JC003641.

874

875 Shokr, M. E. and N. K. Sinha, 1994, Arctic sea ice microstructure observations
876 relevant to microwave scattering, *Arctic*, *47*, 265-279

877

878 Sihvola, A. H. and J. A. Kong, 1988, Effective permittivity of dielectric mixtures,
879 *IEEE Trans. on Geoscience and Remote Sensing*, *26*, 420-429

880

881 Sillars, R., 1937. The properties of a dielectric containing semi-conducting particles of
882 various shapes. *Journal of Institute of Electrical Engineers*, p. 378.

883

884 Thyssen, F., H. Kohnen, M.V. Cowan and G.W. Timco, 1974, DC Resistivity
885 measurements on sea ice near Pond Inlet, N.W.T (Baffin Island), *Polarforschung*, 44,
886 117-126.
887
888 Timco, G.W., 1979, An analysis of the in-situ resistivity of sea ice in terms of its
889 microstructure, *J. Glaciol.*, 22, 461–471.
890
891 Tinga, W.R., W.A.G. Voss, and D.F. Blossey, 1973, Generalized approach to
892 multiphase dielectric mixture theory, *J. Appl. Phys.*, 44, 3897-3902.
893
894 Toyama, Y., F. Nishio and J. Hasegawa, 2001, Characteristics of DC conductivity
895 measurement in sea ice, *Seppyo*, 63, 253-264.
896
897 Vant, M. R., R. O. Ramseier and V. Makios, 1978, The complex-dielectric constant of
898 sea ice at frequencies in the range 0.1-40 GHz, *J. Appl. Phys.*, 49, 1264-1280.
899
900 Wagner, K., 1914. The after effect in dielectrics. *Arch. Electrotech*, 2, 378–394.
901
902 Wakatsuchi, M., and T. Kawamura, 1987, Formation processes of brine drainage
903 channels in sea ice, *J. Geophys. Res.*, 92, 7195-7197.
904
905 Weeks, W.F., 1998, Growth conditions and the structure and properties of sea ice in:
906 *Physics of Ice-Covered seas*, editor M. Lepparanta, pp. 25-104, Springer-Verlag, New
907 York.
908

909 Weeks, W.G., 2010, *On Sea Ice*, University of Alaska Press.

910

911 Wolff, E. W., W. D. Miners, J. C. Moore and J. G. Paren, 1997, Factors Controlling

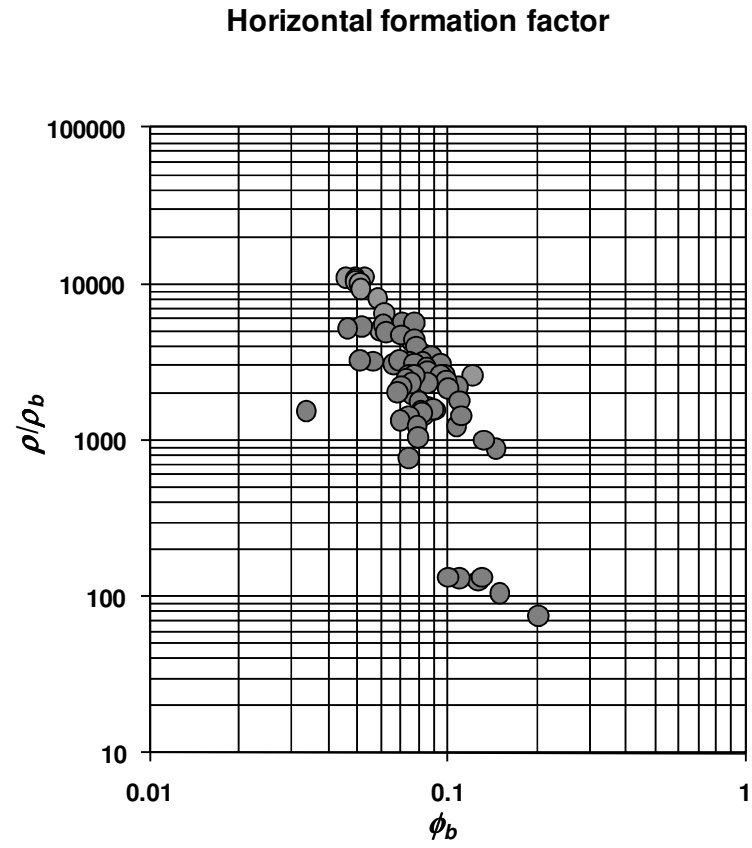
912 the Electrical Conductivity of Ice from the Polar Regions-A Summary, *J. Phys. Chem.*

913 *B*, *101*, 6090-6094.

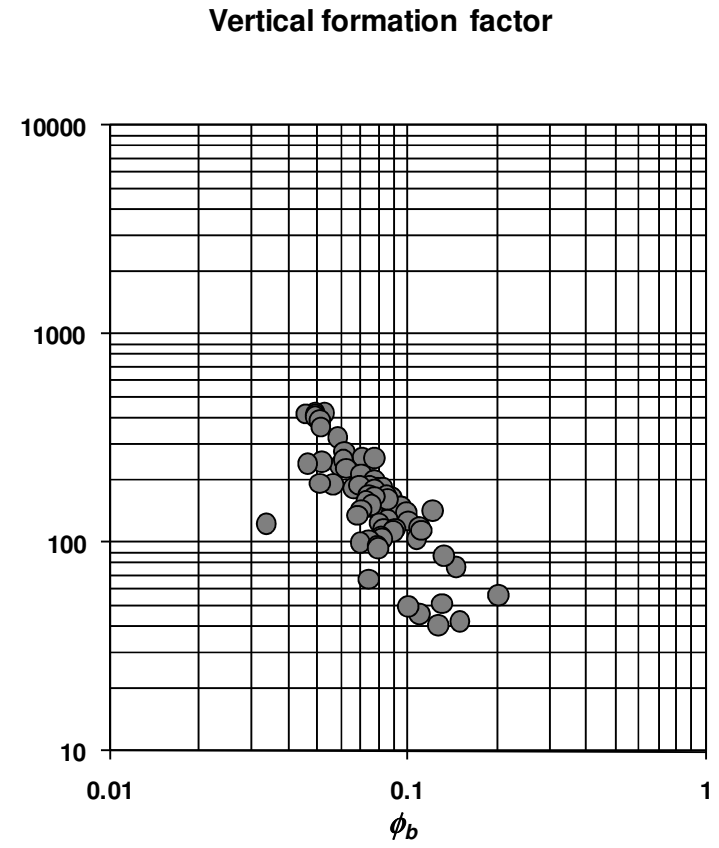
914

ϕ_c	Vertical Formation Factor		Horizontal Formation Factor	
	FF_o	Rms misfit	FF_o	Rms misfit
0.033	4.01	0.534	-	-
0.03	3.27	0.376	-	-
0.024	-	-	0.197	0.455
0.02	2.07	0.249	0.155	0.353
0.01	1.46	0.198	0.101	0.312
0.005	1.25	0.182	0.084	0.311
0.001	1.12	0.173	0.075	0.314

Table 1: Values of FF_o and root mean square misfit for different critical brine volume fractions (ϕ_c) for the fit of functions of the form of equation (24) to the observed formation factor data.



(a)



(b)

Figure 1: Plots of formation factor (ρ/ρ_b) against brine volume fraction (ϕ_b) for (a) horizontal and (b) vertical components of resistivity (Jones et al., 2010) for data from landfast first-year sea ice at Barrow, Alaska.

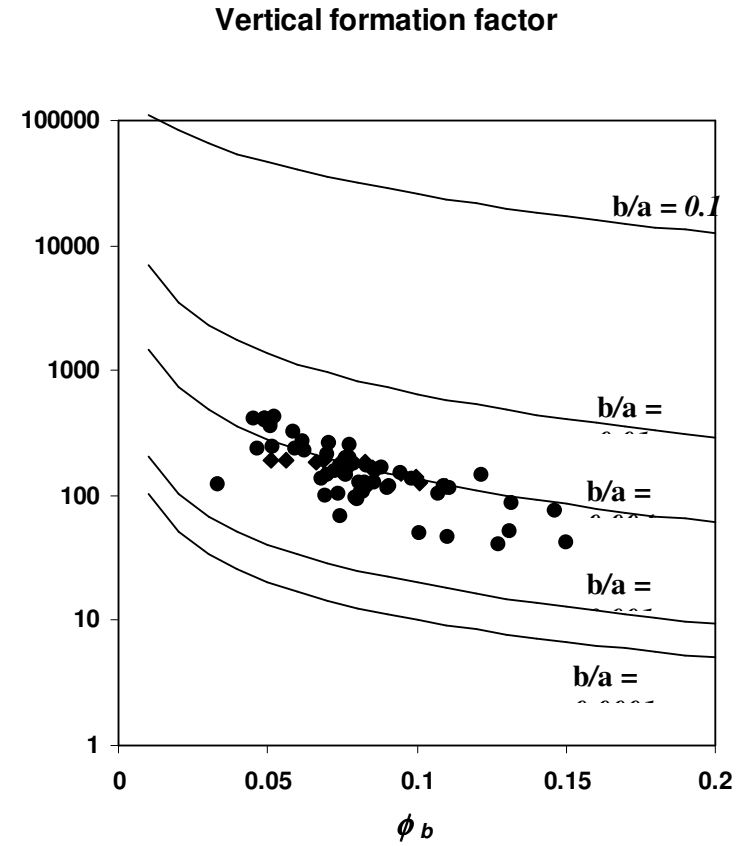
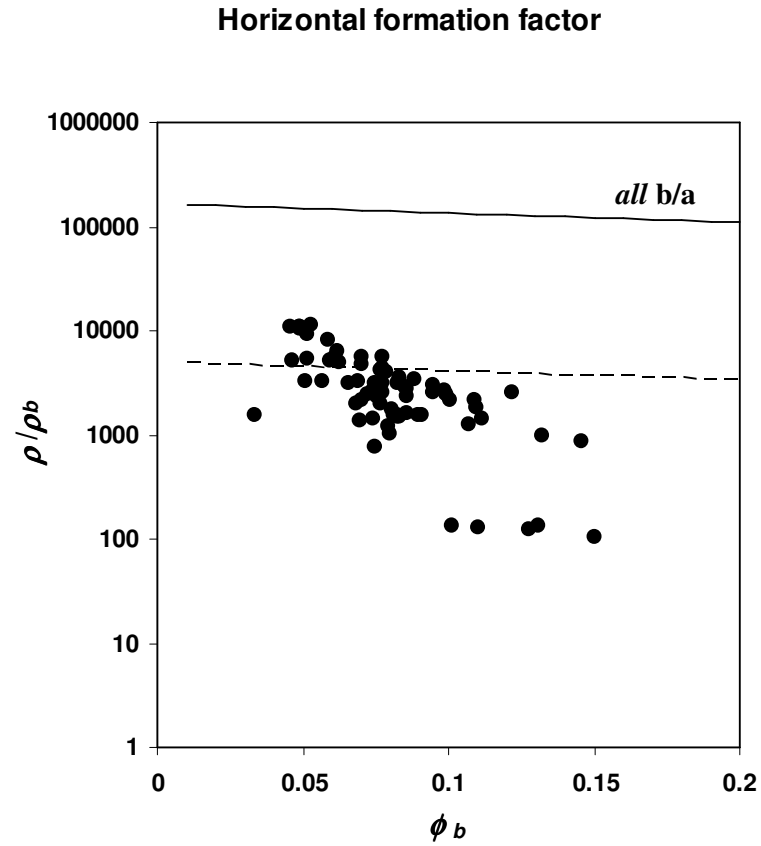


Figure 2: Fit to the formation factor variation with brine volume fraction given by the theory of Tinga et al. (1973) and Vant et al. (1978). Assuming a conductivity of 3×10^{-5} S/m for ice and 5 S/m for brine, predicted values of the vertical formation factor are shown for different ratios of the axes of prolate spheroids (brine inclusions) embedded in an ice matrix. For the horizontal formation factor all ratios b/a give the same curve (solid line). The dashed line shows the result for the horizontal formation factor if an ice conductivity of 0.001 S/m is assumed.

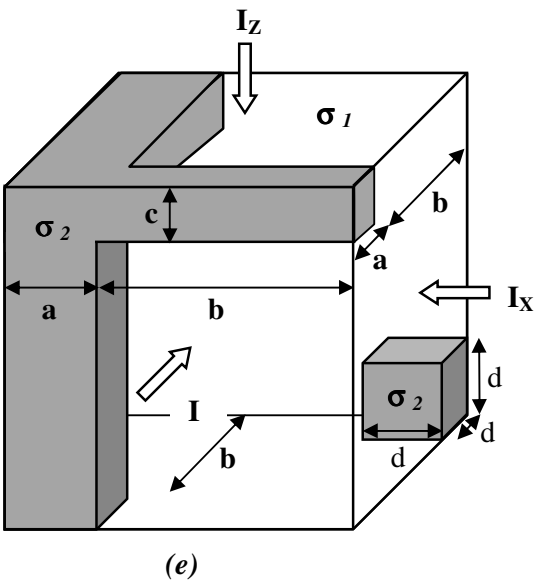
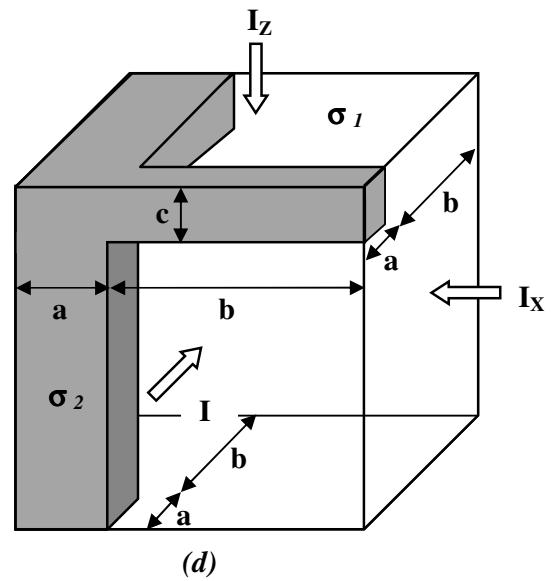
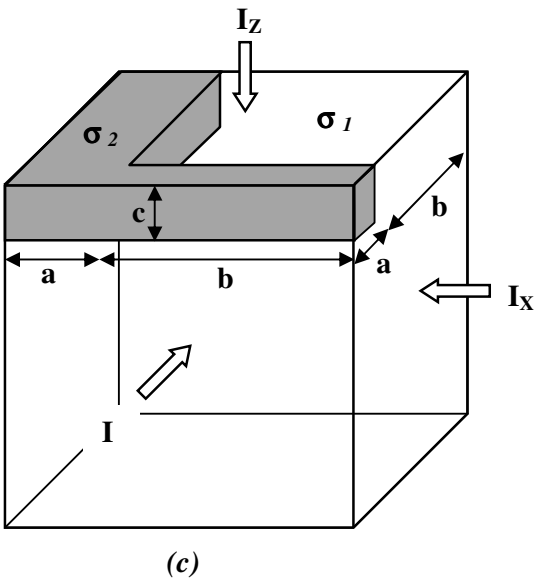
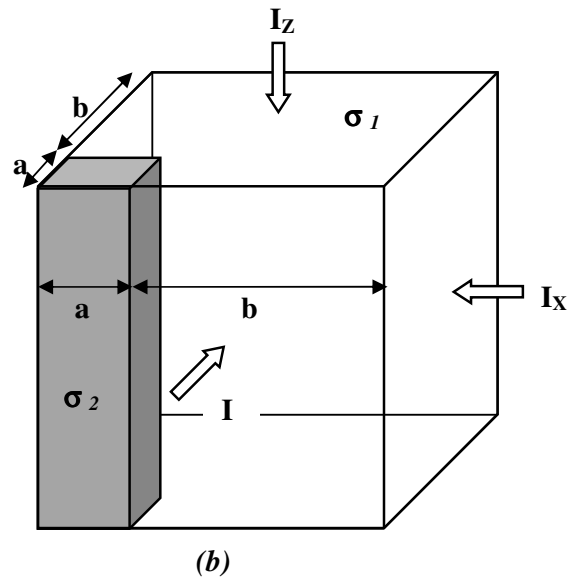
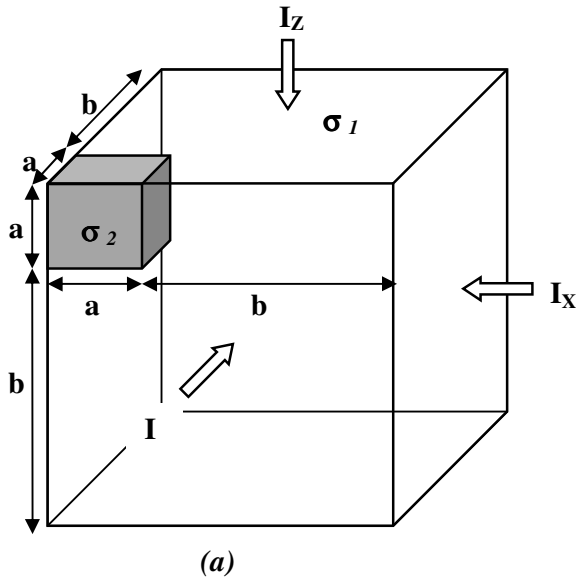


Figure 3: Stages in the development of a structural model that explains the variation of horizontal and vertical formation factors with brine volume fraction. (a) Initial model of isolated brine inclusions in an ice matrix. (b) Model of vertical columns of brine within an ice matrix which yields the correct magnitude of the vertical formation factor. (c) Similar model, with horizontal brine connections, which gives the correct horizontal formation factors. (d) Combination of (c) and (d) which gives the correct formation factors in both horizontal and vertical directions but underestimates the brine volume fraction. (e) Final model with the addition of extra brine inclusions to model (d).

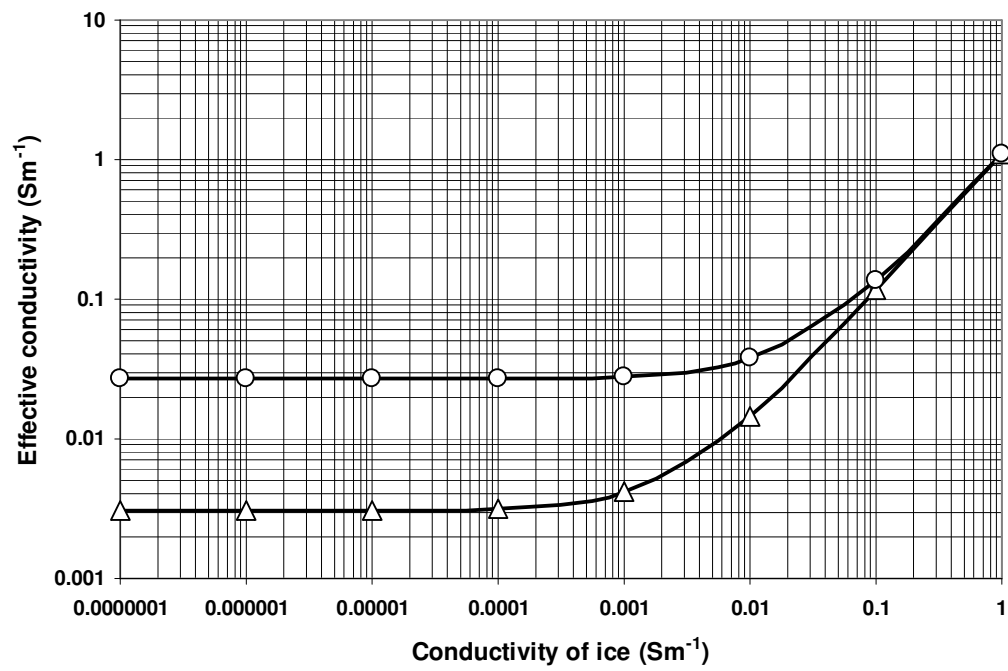


Figure 4: Variation of the effective horizontal (triangles) and vertical (circles) conductivities of model (e) as a function of assumed conductivity of the ice matrix.

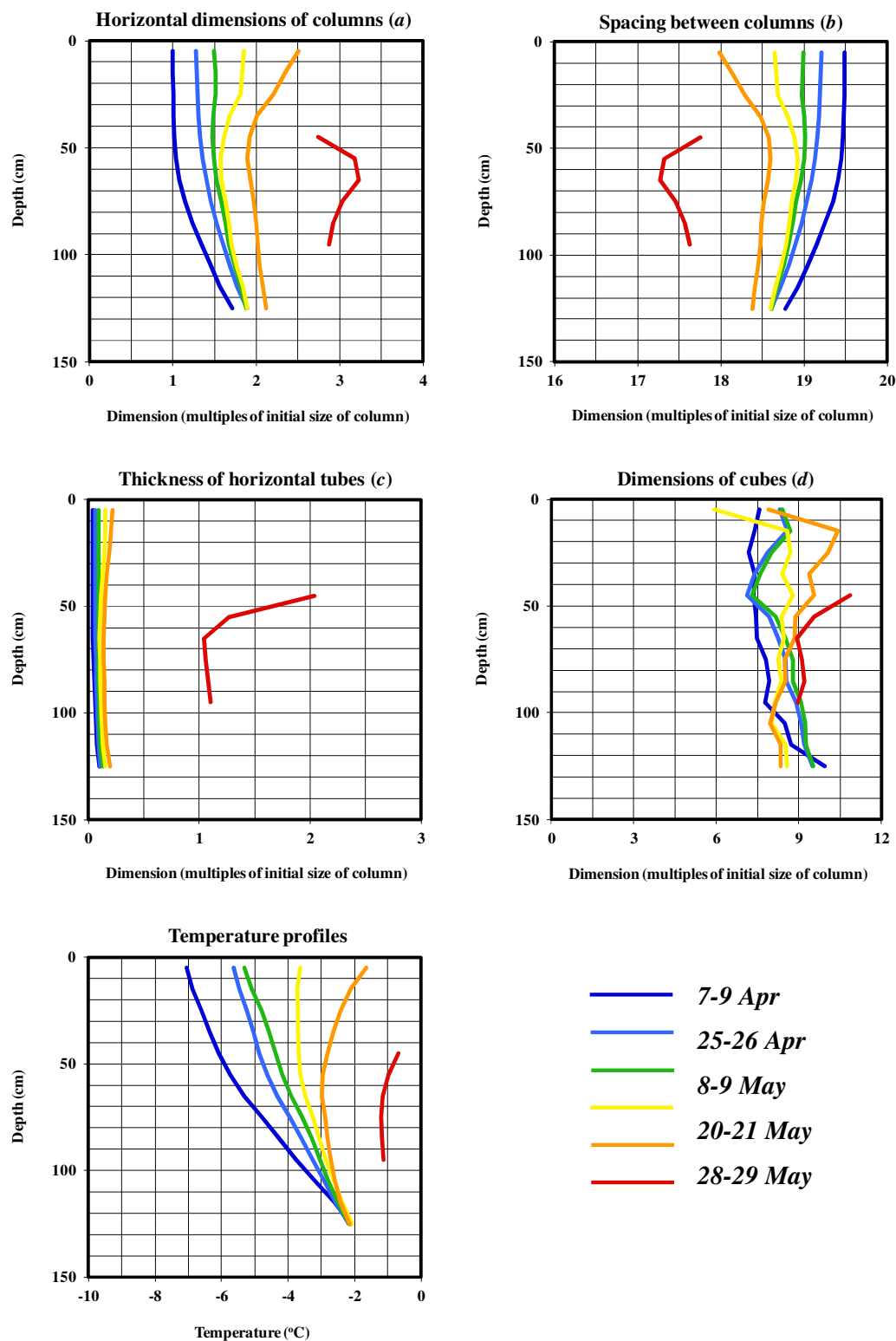


Figure 5: Variation with depth in the ice and time of the dimensions of the structural model shown in Figure 3(e), derived from field measurements of resistivity completed in 2008. Dimensions are relative to the minimum dimension of a . Also shown are the temperature-depth profiles in the ice on each measurement date.

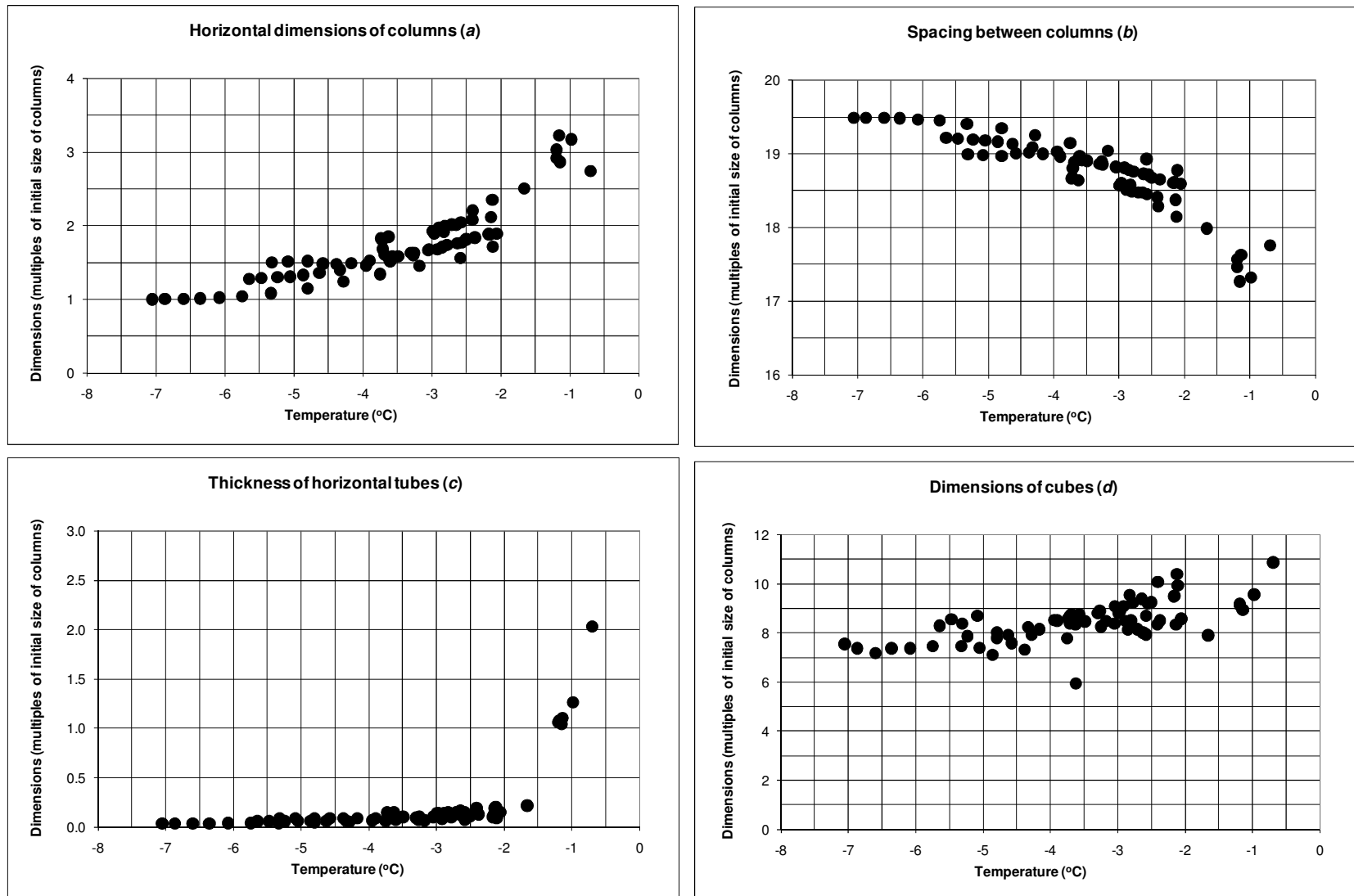


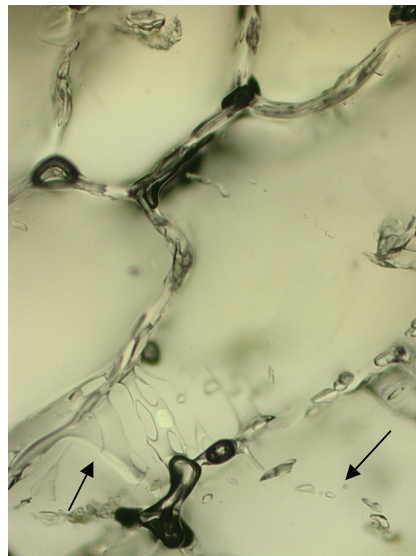
Figure 6: Variation of the relative dimensions a , b , c and d with temperature.



(a)



(b)



(c)

Figure 7: (a) Stratigraphic photograph of part of a core (92 to 137 cm depth) taken on 26 May 2008 near the field site in comparable landfast ice, showing sets of vertical brine channels at roughly 100, 110 and 120 cm depth in the core. (b) Photograph of the bottom of the same ice core (diameter approximately 10 cm) showing ice lamellae separated by narrow brine layers (the latter accentuated by brownish-greenish ice algae). (c) Microphotograph of a vertical thin section (sampled in March 2000) obtained in comparable congelation ice in landfast ice near the 2008 sampling site illustrating brine layers visible in Figure 7(b) at high magnification (height of image approximately 1 mm). Note also the much narrower brine layers and brine tubes (arrowed) connecting the larger layers in the horizontal direction, visible in particular in the bottom part of the image.

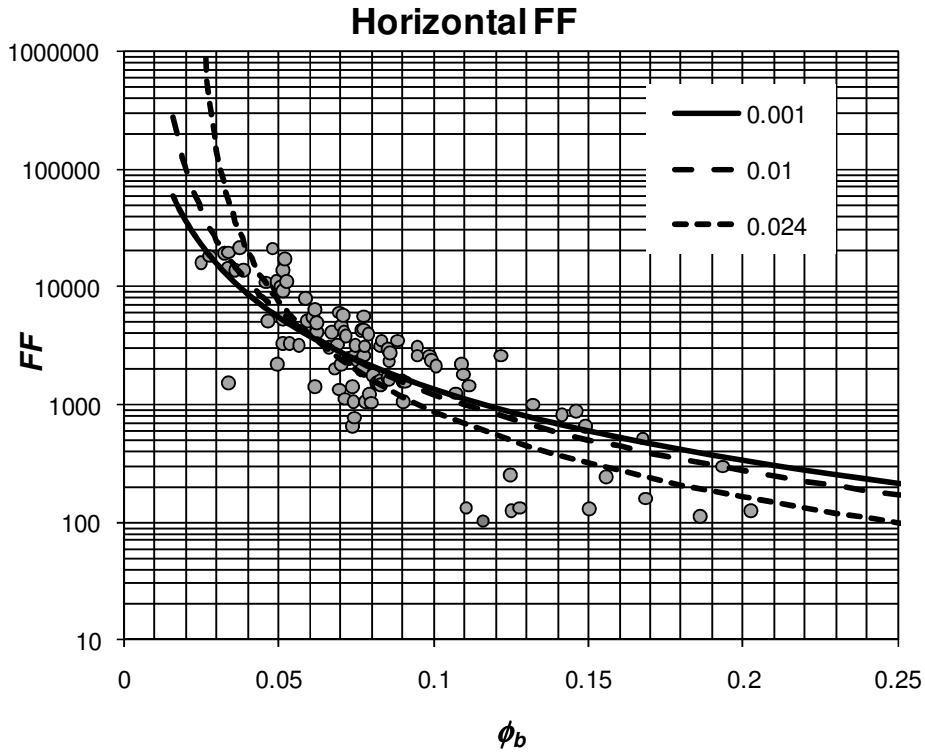
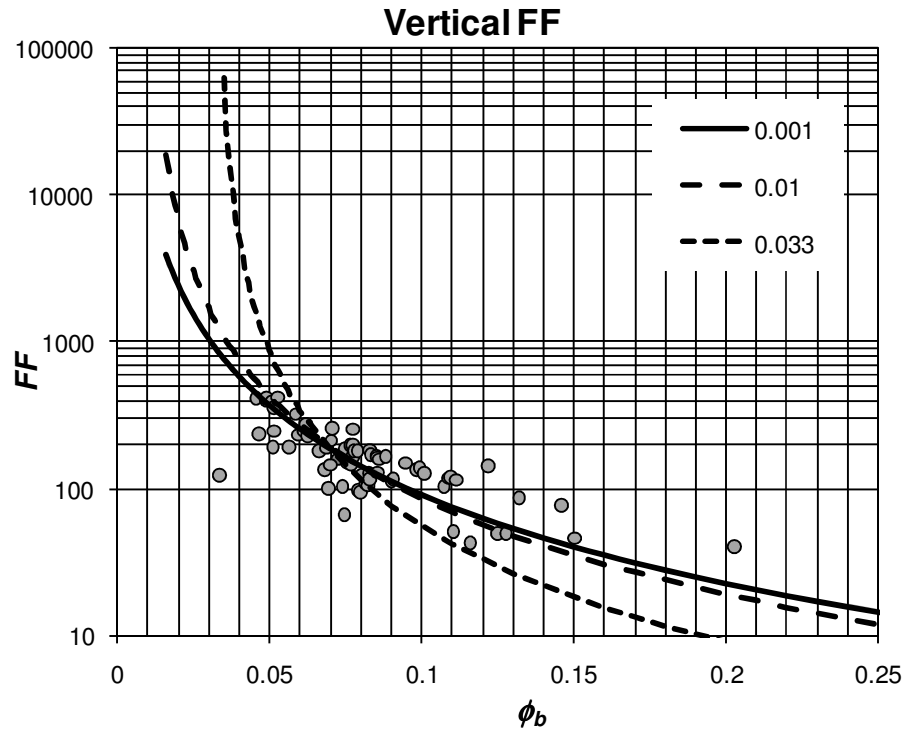


Figure 8: Fits of mathematical expressions of the form of equation (24) to the vertical and horizontal observed formation factor data for critical brine volume fractions as shown in the legends. Corresponding values of the factor FF_o and the rms misfit are as given in Table 1.